PCCP

PAPER

View Article Online
View Journal | View Issue

Published on 11 May 2016. Downloaded by University of California - Berkeley on 27/05/2016 01:21:37.

Cite this: *Phys. Chem. Chem. Phys.*, 2016, **18**, 14644

Tracking dissociation dynamics of strong-field ionized 1,2-dibromoethane with femtosecond XUV transient absorption spectroscopy†

Adam S. Chatterley,[ab] Florian Lackner,[ab] Daniel M. Neumark,[ab] Stephen R. Leone[abc] and Oliver Gessner*[a]

Received 19th April 2016,
Accepted 11th May 2016

DOI: 10.1039/c6cp02598f

www.rsc.org/pccp

Using femtosecond time-resolved extreme ultraviolet absorption spectroscopy, the dissociation dynamics of the haloalkane 1,2-dibromoethane (DBE) have been explored following strong field ionization by femtosecond near infrared pulses at intensities between 7.5×10^{13} and 2.2×10^{14} W cm^{-2}. The major elimination products are bromine atoms in charge states of 0, +1, and +2. The charge state distribution is strongly dependent on the incident NIR intensity. While the yield of neutral fragments is essentially constant for all measurements, charged fragment yields grow rapidly with increasing NIR intensities with the most pronounced effect observed for Br^{++}. However, the appearance times of all bromine fragments are independent of the incident field strength; these are found to be 320 fs, 70 fs, and 30 fs for $Br^{\bullet}$, Br^{+}, and Br^{++}, respectively. Transient molecular ion features assigned to DBE^{+} and DBE^{++} are observed, with dynamics linked to the production of Br^{+} products. Neutral $Br^{\bullet}$ atoms are produced on a timescale consistent with dissociation of DBE^{+} ions on a shallow potential energy surface. The appearance of Br^{+} ions by dissociative ionization is also seen, as evidenced by the simultaneous decay of a DBE^{+} ionic species. Dicationic Br^{++} products emerge within the instrument response time, presumably from Coulomb explosion of triply charged DBE.

Introduction

The interaction of intense laser fields ($>10^{13}$ W cm^{-2}) with molecular systems leads to highly complex dynamics and processes,[1,2] including nonadiabatic multielectron dynamics,[3,4] dissociative ionization,[5,6] Coulomb explosion,[7–9] and high-harmonic generation.[10–12] Simple haloalkanes have served as excellent benchmark systems for studying these interactions.[13–19] Understanding the effect of intense laser fields on molecules has important implications for several areas of fundamental chemistry such as coherent control of bond fission[20,21] and Coulomb explosion imaging.[22,23] In this work, femtosecond extreme ultraviolet (XUV) transient absorption spectroscopy is used to explore the elimination dynamics of Br atoms and ions following strong field ionization (SFI) of 1,2-dibromoethane (DBE, $C_2H_4Br_2$). XUV transient absorption provides the unique capability of simultaneously observing the appearance of both charged and neutral atoms, as well as transient molecular configurations with femtosecond time resolution, from the perspective of well-defined reporter atoms.[24,25]

Mass spectrometry and ion imaging techniques have shown that in strong-field ionized haloalkanes, a great multitude of effects can occur, including elimination of numerous charged fragments,[17,18,21] and in some cases new bond formation.[13,16,26] Recently, transient XUV absorption (TXA) experiments have been performed on two bromoalkanes, dibromomethane (CH_2Br_2)[15] and vinyl bromide (C_2H_3Br),[19] following strong field excitation at intensities around 10^{14} W cm^{-2}. These experiments allow for a unique probe into the dynamics occurring immediately after strong field ionization, extending insight, in particular, into SFI induced dissociation processes. In both experiments, neutral Br atoms were the only atomic fragments produced, although with markedly different timescales: 130 fs and 74 fs for the two spin–orbit configurations in dibromomethane, and 330 fs in vinyl bromide. The presence of additional degrees of freedom and/or a C=C bond appears to dramatically affect the dissociation pathway in vinyl bromide. DBE serves as an intermediate between these two compounds; compared to dibromomethane it possesses a carbon–carbon bond but unlike in vinyl bromide, this is a single bond.

The emergence of cations from strong-field ionized DBE has recently been explored by Sun and co-workers.[16,17] Using velocity

[a] *Chemical Sciences Division, Lawrence Berkeley National Laboratory, Berkeley, California 94720, USA. E-mail: ogessner@lbl.gov*
[b] *Department of Chemistry, University of California, Berkeley, California 94720, USA*
[c] *Department of Physics, University of California, Berkeley, California 94720, USA*
† Electronic supplementary information (ESI) available. See DOI: 10.1039/c6cp02598f

 This journal is © the Owner Societies 2016

Published on 11 May 2016. Downloaded by University of California - Berkeley on 27/05/2016 01:21:37.

map imaging, many product channels were observed in a single-pulse experiment employing a near infrared (NIR) peak intensity of 1.3×10^{14} W cm^{-2}. Significant populations of Br^{++} and Br^{+} ions were produced, along with molecular ions including $C_2H_4Br^{+}$, CH_2Br^{+} and, intriguingly, Br_2^{+} dimers. Some mechanistic detail of the fragment formation was determined from the kinetic energy release and angular distributions of the cationic fragments. It was concluded that $C_2H_4Br^{+}$ ions appear primarily from a dissociative ionization process that includes the loss of a $Br^{\bullet}$ atom, while Br^{+} ions appear from both Coulomb explosion and dissociative ionization processes. Note that these single-pulse mass spectroscopy experiments do not yield dissociation lifetimes and are insensitive to purely neutral dissociation pathways.

Here, femtosecond XUV transient absorption spectroscopy is used to monitor the emergence of each charge state of Br^{n+} ($0 \leq n \leq 2$) fragments produced by SFI in tandem with the appearance and decay of transient DBE^{+} and DBE^{++} molecular configurations. Studying the yields of molecular and fragment species as a function of both time and strong-field intensity reveals correlations that help to disentangle the intricate reaction mechanisms. We find that each charge state of Br^{n+} is produced through a unique dynamical pathway that is independent of the strong-field intensity. Both $Br^{\bullet}$ atoms as well as Br^{+} ions most likely originate from dissociative ionization of DBE^{+}, while Br^{+} production may also be linked to Coulomb explosion. Br^{++} ions are produced within the timescale of the instrument response function, presumably from complex mechanisms including Coulomb explosion of DBE^{+++}. Transient signals associated with ionic molecular peaks are observed that decay with time constants matching those of Br^{n+} product appearance. This suggests that the two dynamical processes are linked, and the dissociation of molecular ions is directly observed.

Methods

The XUV transient absorption setup has previously been described in detail,[19,27] so only an overview is given. 1,2-Dibromoethane (Sigma-Aldrich, 98%) is loaded into a stainless steel sample reservoir, connected by stainless steel tubing to a ceramic sample cell. To produce sufficient vapor pressure of DBE, the reservoir, sample delivery line, and sample cell are all heated to $\sim$70 °C, corresponding to a reservoir vapor pressure of 82 Torr. The pressure inside the sample cell is held at $\sim$2 Torr using a needle valve. The sample cell is a cylinder with 1 mm internal diameter that has 750 μm holes drilled into both sides to allow light to be transmitted. Spent DBE is captured using a liquid nitrogen cryotrap.

The primary light source for the experiment is a Ti:sapphire based femtosecond laser system (3 kHz, 780 nm central wavelength, 3.3 mJ pulse^{-1}, $\sim$35 fs pulse length). Half the pulse energy is used for the strong field NIR pump pulse, and the other half is used for the XUV probe pulse. The NIR pump pulse is attenuated using a half-wave plate and a thin film polarizer, allowing for continuous variation of the pump intensity without changing its spatial characteristics. The attenuated beam is focused into the sample chamber with an *f*/40 lens. This results in a focused intensity varying from approximately 7.5×10^{13} W cm^{-2} to 2.2×10^{14} W cm^{-2}, which is determined using a power meter and a CCD beam profiler. The power density calibration is confirmed using the ratio of Xe^{+} to Xe^{++} yields produced by SFI.[28]

The XUV probe pulse is produced using high-harmonic generation (HHG) by focusing 1.6 mJ of NIR light into a semi-infinite gas cell filled with 80 Torr of neon gas as the non-linear medium. The resultant high order harmonics are quasi-continuous and span a photon energy range of approximately 50 to 73 eV. A 300 nm thick Al foil is used to block the NIR driving pulse that co-propagates with the high-harmonic light. The XUV probe beam is focused into the sample cell using a toroidal mirror, crossing the NIR pump beam at a 1° angle. A variable line space grating disperses the XUV light that emerges from the interaction volume onto an X-ray CCD camera, which records the transmitted XUV spectrum. To protect the toroidal mirror and X-ray CCD from DBE vapor, two additional 200 nm thick Al filters are used to isolate both sides of the interaction chamber from the rest of the vacuum system.

The time delay between the pump and probe pulses is varied using a motorized, computer-controlled delay stage. The spatial pump–probe overlap is optimized by maximizing the 4d absorption signal of Xe^{+} ions produced by SFI. The appearance of this signal also provides time zero of the pump–probe delay and an instrument response function (IRF) of 40 fs full-width-at-half-maximum (FWHM). Energy calibration of the spectrometer is performed using the characteristic 4d absorption lines of both Xe atoms and Xe^{+} ions, which are also used to determine the spectral resolution of $\sim$100 meV (FWHM). Note that this is a significant improvement from our previous work,[19] due to a new grating and XUV camera. The probe XUV beam waist (25 μm) is significantly smaller than that of the NIR pump beam (85 μm) and the Rayleigh ranges of both beams are at least an order of magnitude longer than the interaction region; hence the volume probed stays essentially constant as intensity is varied.

All transient absorption spectra are referenced to the XUV spectrum recorded with the pump laser blocked. An optical chopper is used to block the pump laser at 4 Hz and the data acquisition is synchronized to the chopper. Thus, each camera exposure records 750 laser pulses under alternating pump-on/pump-off conditions. This allows the reference spectrum to be acquired almost simultaneously with the signal spectrum, minimizing the impact of low frequency temporal variations in the high-harmonic spectrum on the transient absorption spectra. Transient absorption is reported in ΔOD (change in optical density), defined for a given photon energy E and pump–probe delay t as $\Delta OD(E,t) = \log_{10}(I_{reference}(E)/I_{signal}(E,t))$. The intensities I_{signal} and $I_{reference}$ refer to the amount of transmitted XUV light when the pump beam is on and off, respectively. The spectrum for each pump–probe delay and each pump intensity is an average of 30 scans, with 5 s of exposure (2.5 s pump on, 2.5 s pump off) per scan. The statistical scatter of the 30 scans is used to derive the reported error bars, which represent 68% confidence intervals. The static XUV absorption

Published on 11 May 2016. Downloaded by University of California - Berkeley on 27/05/2016 01:21:37.

spectrum as a function of photon energy E is reported as optical density $OD(E) = \log_{10}(I_0(E)/I_{sample}(E))$, where I_{sample} and I_0 are the transmitted XUV intensities with and without DBE in the sample cell, respectively.

Density functional theory (DFT) calculations using the QChem 4.2 package[29] were performed to calculate dissociation energies. The B3LYP functional and auc-cc-pVDZ basis set[30,31] were used throughout. For each dissociation product, the geometry was optimized, and a vibrational frequency calculation was performed to ensure that the configurations represent true minima.

Results

1. Long time delay XUV absorption spectra of strong field excited DBE

The static XUV absorption spectrum of DBE is plotted as a dotted curve in Fig. 1a. A single bimodal feature with maxima at 70.6 eV and 71.5 eV, along with a slight linear background are the only structures within the entire energy range of the experiment (50 eV $< h\nu <$ 73 eV, shown only above 64 eV). A nonlinear least squares fit using two Gaussian shaped peaks and a linear slope reproduces the spectrum well (red solid line). By comparison with other bromoalkanes, we assign the two peaks of the feature to the two spin–orbit contributions from excitations of Br $3d_{5/2,3/2}$ electrons into the lowest unoccupied molecular orbital (LUMO), which is of C–Br σ^* character.[15,32,33] The slightly sloped background is a contribution from excitations of valence electrons into the continuum.

Following strong field excitation of DBE, a significantly more complex spectrum is observed in the bromine 3d region. Fig. 1b shows four spectra, each obtained 1 ps after arrival of the pump pulse, for four different strong field intensities, ranging from $\sim 7.5 \times 10^{13}$ W cm^{-2} to $\sim 2.2 \times 10^{14}$ W cm^{-2}. A large number of sharp peaks are observed below 70 eV, and a broad depletion feature extends from 70 to 72 eV. Despite the complexity of the spectrum, virtually all sharp peaks can be readily assigned to atomic fragments as indicated in Fig. 1c, while broader peaks belong to molecular species.[34] Fig. 1c shows the result of a nonlinear least squares fit (dark blue) to the spectrum recorded at the highest pump intensity (thick yellow). The fit is composed of a series of narrow ($\leq$200 meV) Gaussian functions distributed across the entire spectral range, a broad Gaussian peak located at $\sim$66 eV, and a broad, bimodal depletion feature between 70 and 72 eV. This depletion corresponds very well to the static absorption spectrum of unperturbed DBE (Fig. 1a), and we assign it to the depletion of the parent molecule population upon ionization. All sharp peaks below 70 eV are centered within $\pm$50 meV of known atomic Br^{n+} (n = 0, 1, 2) peak positions, and only the peak intensities and widths ($\leq$200 meV FWHM) are varied during the fit procedure. Note that the small deviations of the absorption energies from the literature values are within the energy resolution of the experiment ($\sim$100 meV). The fit results and spectroscopic assignments for the atomic lines are tabulated in the ESI.†

The peaks at 64.4 eV and 65.0 eV (yellow) are associated with two spin–orbit split transitions in neutral Br$^\bullet$ atoms.

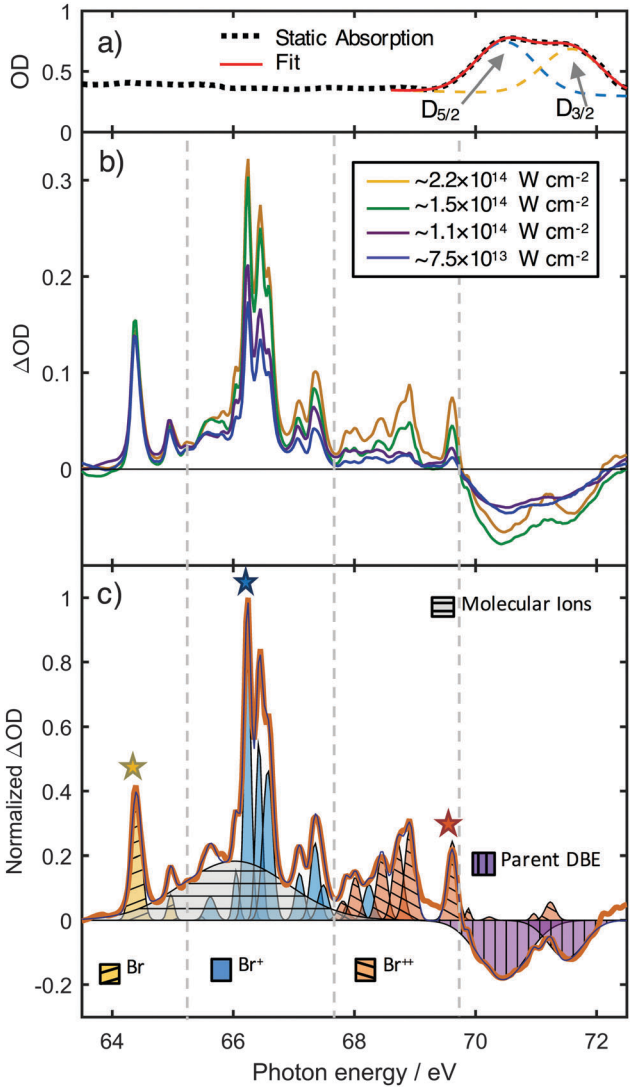

Fig. 1 (a) Static XUV absorption spectrum of DBE. The feature at 71 eV has been fit using two Gaussian shaped peaks, representing the two spin–orbit split excitations from the Br $3d_{3/2,5/2}$ levels to the lowest unoccupied molecular orbital, along with a linear background to account for valence absorption. (b) XUV transient absorption spectra of DBE, recorded 1 ps after excitation with 4 different NIR pump pulse intensities. Four spectral regions are observed, corresponding to the emergence of Br, Br^+, and Br^{++} fragments, as well as the depletion of neutral DBE. The regions are indicated by vertical dashed lines and distinct peak patterns in (c), which shows a fit (dark blue) of the $\sim 2.2 \times 10^{14}$ W cm^{-2} spectrum (thick yellow). The experimental and model curves in (c) are almost indistinguishable. Gaussian functions corresponding to the literature peak positions have been used to describe the Br$^\bullet$ (yellow), Br^+ (blue) and Br^{++} (orange) signals. Broad molecular features around 66 eV are represented by a single gray Gaussian, and the depletion of the parent molecular signal is represented by two purple Gaussians. Colored stars indicate the peaks chosen to represent the population of each charge state of Br in the analysis below.

Another low intensity peak is expected at 65.4 eV, however in our spectra this feature appears to be obscured. The Br$^\bullet$ features show no dependence on the pump pulse intensity (Fig. 1b). Between 66 eV and 67.7 eV, several sharp peaks are visible that are associated with absorption of Br^+ ions (blue). The large

 This journal is © the Owner Societies 2016

Published on 11 May 2016. Downloaded by University of California - Berkeley on 27/05/2016 01:21:37.

number of peaks observed indicates that Br^+ is produced in a wide range of states. The singly charged ion peaks increase modestly with strong field intensity. Br^{++} transitions appear higher in energy, and these account for the structure observed from around 68 eV to 70 eV (orange). These peaks are highly dependent on the pump pulse intensity, increasing approximately 7-fold over the range of intensities used. A quantitative plot of the intensity dependence of the three charge states of Br atoms is available in the ESI.† Between 70.8 eV and 71.4 eV, overlapping the parent depletion, another strongly field-dependent structure is observed. Cummings and O'Sullivan predicted two Br^{++} peaks to be located in this energy range; thus, we assign these features also to Br^{++}. To our knowledge, this is the first experimental observation of these lines in the 3d absorption spectrum of Br^{++}. The structure is a broad doublet, with peaks at 71.0 and 71.2 eV, however the peak intensities are insufficient to describe the features in more detail. From the predictions of Cummings and O'Sullivan we can tentatively assign the two peaks to $^2P_{1/2} \rightarrow (^1S)\,^2D_{3/2}$ and $^2D_{5/2} \rightarrow (^1S)\,^2D_{5/2}$ transitions, respectively.

The atomic lines and parent depletion features alone are insufficient to accurately model the absorption spectrum at long time delays. To account for additional spectral contributions from molecular ions, a single broad Gaussian function centered at ~66 eV (gray) has been included in the fit in Fig. 1c. Since velocity map imaging (VMI) experiments with similar strong field excitation revealed a large variety of Br-containing ionic molecular fragments,[16,17] we assign this feature to a collection of long-lived Br-containing molecular fragments. We note that a signature of the dimer fragment Br_2^+ (as observed by Wu *et al.* using mass spectrometry), which would be most visible around 66.7 eV, cannot be discerned in our spectra, most likely due to its low yield compared to the intense atomic peaks. In the long time limit shown in Fig. 1b and c, the atomic lines obscure the molecular features; however, a combination of short delay spectra and dynamic trends allow us to analyze the molecular signals as well, as outlined below.

2. Time dependence of XUV absorption spectrum

The XUV absorption spectrum as a function of pump–probe delay at a pump intensity of $\sim 1.5. \times 10^{14}$ W cm^{-2} is presented in Fig. 2. At $t = 0$, prompt depletion of the neutral DBE signal between 70 and 72 eV is observed. This is accompanied by the instantaneous appearance of two short-lived broad features, located around 66 eV and 69 eV. These features decay in less than 100 fs and are replaced by the atomic ion lines described above. In XUV transient absorption spectroscopy, short-lived broad features like these tend to be associated with molecular ions,[25,35] hence these transient features can be assigned to DBE^+ and/or DBE^{++} molecular ions, rapidly dissociating into atomic species. Fig. 2 nicely demonstrates the clear distinction between dynamics of transient molecular and emerging fragment species enabled by time-resolved inner-shell absorption spectroscopy, providing unique insight into molecular transformations induced by SFI from a local perspective.

At lower photon energies, ~64–65 eV, the neutral $Br^\bullet$ peak rises on a markedly slower time scale compared to the rapidly appearing charged atomic ions, growing in gradually over the course of hundreds of femtoseconds.

Discussion

1. Transient molecular features

We shall first discuss the broad transient features visible at short delays. Fig. 3 shows the transient spectrum recorded at $t = 0$ with $\sim 1.5 \times 10^{14}$ W cm^{-2} pump intensity (black, thick), in comparison with the spectrum at 1 ps pump–probe delay (blue, thin). A broad doublet feature appears around time zero at low energies with maxima at 65.7 and 66.3 eV. Due to its

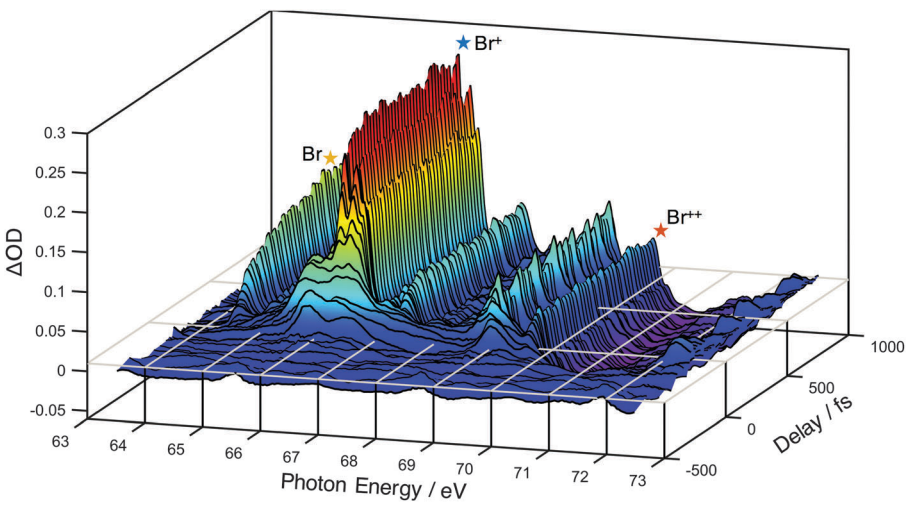

Fig. 2 Waterfall representation of transient XUV absorption spectra recorded with a NIR pump pulse intensity of $\sim 1.5 \times 10^{14}$ W cm^{-2}. At $t = 0$, prompt depletion of the parent molecular feature between 70 and 72 eV is accompanied by the instant appearance of broad transient molecular features below 70 eV, which later decay to produce sharp atomic lines. The peaks chosen to derive the dynamics of each charge state of Br in the figures below are indicated by stars.

Published on 11 May 2016. Downloaded by University of California - Berkeley on 27/05/2016 01:21:37.

immediate appearance within the instrument response time and the broad spectral shape, an intuitive assignment for this feature is the excitation of Br 3d electrons into the highest occupied molecular orbital (HOMO) hole of strong-field ionized DBE^+ cations. Comparison with transient XUV absorption spectra of related Br compounds supports this hypothesis: in both $C_2H_3Br^+$ and $CH_2Br_2^+$ the Br 3d to HOMO hole transitions were found to lie between 66 and 68 eV, suggesting a similar spectral assignment for DBE in this energy range.[15,19] The 0.6 eV energy difference between the two peak maxima, however, is much less than the characteristic Br 3d spin–orbit splitting of ~1 eV; hence we cannot simply assign the double-peak as a spin–orbit feature. Photoelectron spectra of DBE show that the splitting between the ground (π hole) and first excited (σ hole) ionic states is only about 0.5 eV. This suggests that the doublet feature near 66 eV may be composed of Br 3d electron transitions into both HOMO (π) and HOMO−1 (σ) vacancies. Applying this picture, the peak at 65.7 eV is assigned to core-to-valence absorption within the first excited state of the DBE^+ ion, *i.e.* excitation of Br 3d electrons into a HOMO−1 hole. The second spin–orbit component of this peak is presumably superimposed with the HOMO hole peak at 66.3 eV. The second spin orbit component of the HOMO hole feature is visible as a kink in the spectrum at 67.3 eV, and it likely extends out to ~68 eV. Additional intensity is visible at lower photon energies, around 64–65 eV, suggesting further electronic or vibrational excited states of DBE^+, however the intensity is insufficient for any firm assignments to be made.

The feature at 69 eV can be assigned to the DBE^{++} dication by similar arguments to those above: the $CH_2Br_2^{++}$ dication spectrum has a maximum at 68.9 eV,[15] and $C_2H_3Br^{++}$ has a maximum at 68.7 eV.[19] A second spin–orbit maximum should also be present, at around 70 eV, but the strong bleach signal of the parent DBE molecule likely obscures this. Neither DBE^+ nor DBE^{++} have been observed in strong field ionization mass spectrometry experiments,[16,17] supporting the assignment of both of these very short lived features to intact molecular cations that rapidly dissociate to give atomic Br^{n+} fragments.

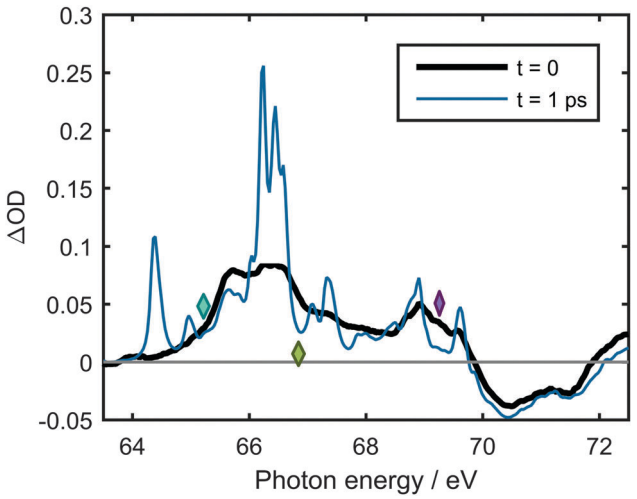

Fig. 3 Transient XUV absorption spectrum recorded with a NIR intensity of ~1.5 × 10^{14} W cm^{-2} at t = 0 (black) in comparison with the spectrum recorded at a pump–probe delay of 1 ps (blue). Broad, short-lived molecular features around 66 and 69 eV dominate the t = 0 spectrum and evolve into the sharp features of neutral and ionic Br^{n+} fragments at long time delays. The energies used for tracking the dynamics of the short-lived species are indicated by diamonds.

2. Quantitative description of dynamics

The time dependent yields of the three different charge states of Br atoms dissociating from DBE after excitation with three different strong field intensities are shown in Fig. 4a–c. The most intense peak from each charge state (indicated by stars in Fig. 1c and 2) has been used to track the dynamics, which minimizes contamination from overlapping peaks. These peaks correspond to transitions involving the ground state configurations of each charge state ($^2P_{3/2}$, $^3P_2$ and $^4S_{3/2}$ for $Br^\bullet$, Br^+ and Br^{++}, respectively), although in the case of Br^{++} there are many overlapping lines, which means the assignment is not definitive (see Table S3 in the ESI†).

All signals are normalized to an asymptotic intensity of 1. It is immediately apparent that although the relative yields of

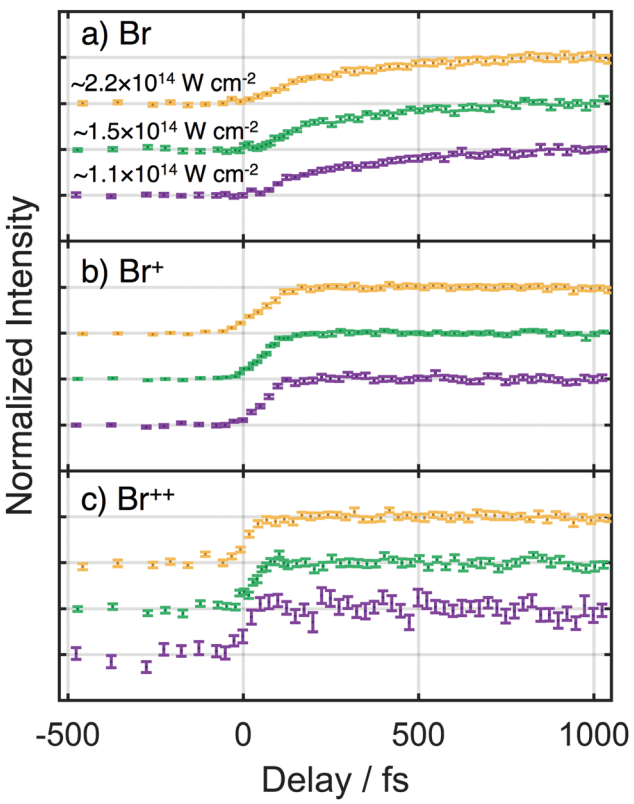

Fig. 4 (a–c) Normalized intensities of the most intense peaks associated with different charge states n = 0, 1, and 2, respectively, of Br^{n+} atoms, at three different NIR pump intensities as indicated. Successively higher charged atoms depart within shorter time scales. For each particular charge state, however, the time scale for dissociation is unaffected by the NIR pump intensity. Error bars are 68% confidence intervals, derived statistically. All curves have been normalized to an equal asymptotic intensity and the three curves in each panel are offset vertically for improved clarity.

This journal is © the Owner Societies 2016

Published on 11 May 2016. Downloaded by University of California - Berkeley on 27/05/2016 01:21:37.

fragments are strongly dependent on the pump pulse intensity (Fig. 1b and Fig. S1, ESI†), the dynamics of their appearance remain essentially unchanged. Each charge state of Br, however, appears on a very different time scale. Neutral Br• atoms emerge over hundreds of femtoseconds while Br^+ ions appear much faster, in tens of femtoseconds. Faster still are the Br^{++} ions, whose appearance is essentially limited by the instrument response ($\sim$40 fs).

Modeling the transients of Fig. 4 by exponential rise functions quantifies the different appearance times related to different Br^{n+} charge states. Fig. 5a shows the normalized Br^{n+} transients recorded with $\sim 2.2 \times 10^{14}$ W cm^{-2} pump intensity (colored symbols) along with fits to basic exponential rise functions ($\propto 1 - \exp(t/\tau)$ for time delays t and a rise time τ), convoluted with the 40 fs (FWHM) Gaussian instrument response (black solid lines). All three traces are described very well by the fits, and the decrease in appearance times as the charge state increases is readily apparent on a qualitative level. The time constants derived from the fits, at all three measured intensities, are presented in Table 1. The fit results confirm that as excitation intensity varies, negligible change is observed in the dynamics. This suggests that only one dissociation mechanism is dominating for each charge state, and a single description should adequately describe the appearance of Br^{n+} fragments at all excitation intensities employed in the experiment.

The dynamics of the transient molecular DBE^{n+} species (Fig. 3) are analyzed in a similar fashion as those of the Br^{n+} fragments. Although the intense atomic lines, which are dispersed throughout the spectrum, make it difficult to completely isolate the molecular signals, gaps in the atomic spectra permit sampling the dynamics of transient molecular species. These gaps are indicated by diamonds in Fig. 3, and appear at 65.3 eV, 66.9 eV, and 69.2 eV. Note that the window at 65.3 eV nominally overlaps a neutral Br• peak, making assignments based on this window necessarily more tenuous – this window was selected because of a strong decaying signal observed there, rather than a definitive spectral assignment. On the other hand, the windows at 66.9 eV and 69.2 eV overlap with the broad features visible in the spectrum at $t = 0$ (Fig. 3), which were previously assigned as DBE^+ and DBE^{++} features, so these are considered more reliable. Fig. 5b–d show the transients associated with $\sim$10–20 meV wide energy integration ranges around the nominal values above, recorded at a NIR intensity of $\sim 2.2 \times 10^{14}$ W cm^{-2} (colored symbols). In all three cases, the data show an instantaneous rise at $t = 0$ followed by a decay to a non-zero baseline. The rate of decay, however, differs significantly between the three signals, indicating that each window is sampling a separate transient species. At a qualitative level, the decay rates of the transients appear to mirror the appearance rates of the atomic species in the corresponding spectral regions. This agreement lends some support to our assignment of these integration windows as molecular species that decay to Br atoms in various charge states.

Since the dynamics of each molecular transient appear to be linked to those of the atomic fragments, fits were performed using the atomic rise times as fixed parameters. All three transients have been modeled by the sum of an exponential decay whose lifetime matches the corresponding atomic appearance time ($\propto \exp(-t/\tau)$ for time delays t and atomic rise time τ),

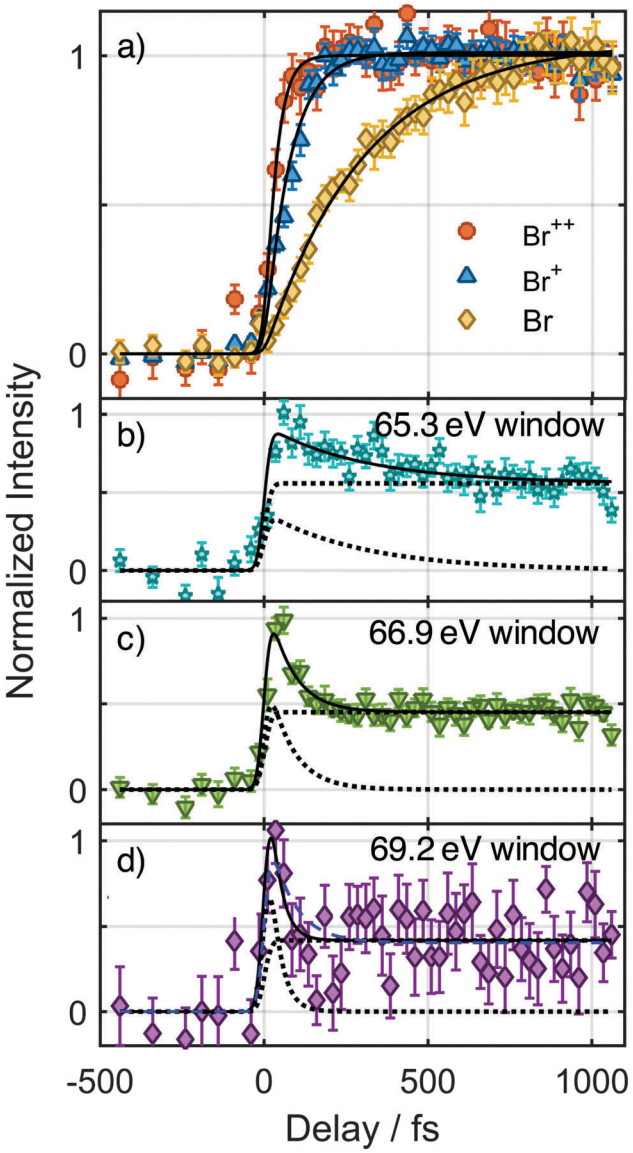

Fig. 5 (a) Modeling the dynamics of the strongest peaks of the three different charge states of Br atoms emerging after strong field ionization at $\sim 2.2 \times 10^{14}$ W cm^{-2}. Each curve was fit using an exponential rise function, convoluted with the instrument response function. (b) Dynamics in the window at 65.3 eV, see text for possible assignments. The experimental curve is fit using a combination of an IRF limited exponential rise, and an exponential decay function with a time constant equal to that derived for the appearance of the Br• atoms. Only the relative contributions of the two components are allowed to vary in the fit. The two contributions are shown by dotted curves, and their sum is shown by a solid curve. (c) Modeling the transient overlapping the DBE^+ signal at 66.9 eV, using the same methodology as in (b), but using the time constant derived for Br^+ production to describe the decaying signal fraction, see text for possible assignments. (d) Fit to the transient overlapping the DBE^{++} signal at 69.2 eV, using the same decay time scale as the appearance time of Br^{++}. Also visible as a blue dashed curve is a fit using the Br^+ time constant, see text for possible assignments.

Published on 11 May 2016. Downloaded by University of California - Berkeley on 27/05/2016 01:21:37.

Table 1 Time constants for the production of Br^{n+} with three different NIR pump intensities. The molecular decay transients have been fit using these same time constants (Fig. 5b–d)

Intensity/W cm^{-2}	$\tau_{Br^{\bullet}}$/fs	$\tau_{Br^{+}}$/fs	$\tau_{Br^{++}}$/fs
$\sim 1.1 \times 10^{14}$	313 ± 80	55 ± 20	≤ 28
$\sim 1.5 \times 10^{14}$	333 ± 90	71 ± 15	29 ± 20
$\sim 2.2 \times 10^{14}$	302 ± 75	74 ± 15	32 ± 20

and a step function, both convoluted with a 40 fs (FWHM) Gaussian. The decay function represents the disappearance of transient molecular species, while the step function accounts for long-lived species that also appear instantly at time zero but do not decay within the time scale of the experiment. The only free parameter in these fits (apart from an arbitrary overall amplitude) is the relative contribution of the two functions. In all three cases, these one parameter fits reproduce the data remarkably well, supporting a dynamical link between the molecular transients and the Br^{n+} fragments. We shall now consider the dynamics associated with each charge state of Br^{n+} in more detail.

3. Origin of Br• fragments

Br• fragments are produced within 320 fs, and the yield of the Br• atoms has saturated already at a NIR intensity of $\sim 7.5 \times 10^{13}$ W cm^{-2} (Fig. 1b). This dissociation lifetime is significantly longer than might be anticipated for a direct dissociation process on a repulsive state.[36,37] Therefore, we assign this lifetime to dissociation of DBE^+ ions from a shallow potential energy surface. In the velocity map imaging experiments performed by Wu *et al.*, processes leading to both Br• and Br^+ fragments from charged DBE species were explored.[16,17] $C_2H_4Br^+$ fragments were primarily formed with zero excess kinetic energy, indicating that these fragments arose from a dissociative ionization (DI) scheme by loss of Br• rather than Coulomb explosion involving multiple charged fragments. In order to better understand the energetics of this dissociative ionization (DI) process, we have performed *ab initio* calculations using DFT. Fig. 6 shows vertical ionization energies of the parent DBE molecule (left) along with the total energies of several single bromine atom elimination channels (right), calculated at the B3LYP/aug-cc-PVDZ level of theory. The most stable gas phase structure of $C_2H_4Br^+$ (the co-fragment in a DI mechanism) is the bromonium ion, a stable triangular cyclic species.[38–41] Our calculations show that the optimized geometry of the bromonium ion and Br• fragment is only 0.5 eV higher in energy than the ground state DBE^+ ion.

Photoionization mass spectrometry experiments found the appearance energy of $C_2H_4Br^+$ to be 10.53 eV, just 0.2 eV higher than the DBE ionization potential (IP, 10.35 eV).[39] This is in reasonable agreement with our DFT calculations, and shows that there is almost no barrier to Br• loss. Indeed, as photoionization energy is increased, Br• loss rapidly becomes the dominant fate of DBE^+, outcompeting intact DBE^+ ions 3 : 1 at an energy 1 eV above the DBE IP. The propensity for Br• loss can in part explain why no evidence of intact DBE^+ parent ions have been found following SFI,[16,17] as an excess energy corresponding

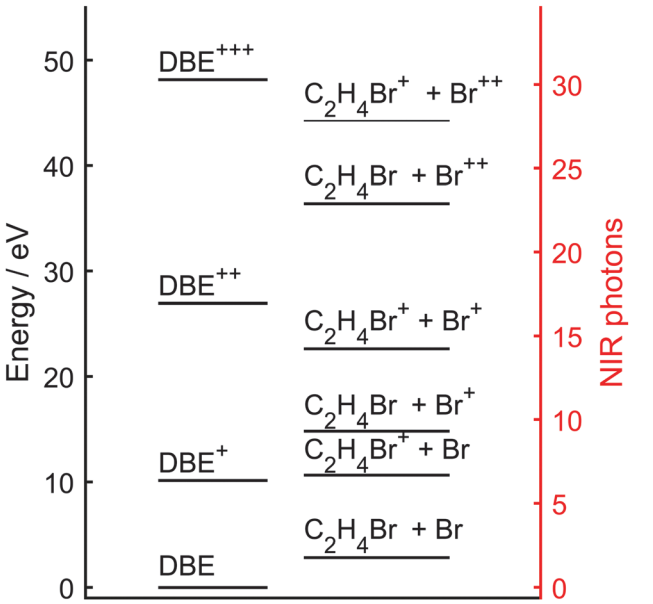

Fig. 6 Calculated energies for relevant ionization and dissociation pathways of DBE. Levels on the left are calculated vertical ionization energies. Levels on the right are calculated total energies of various fragmentation products. Dissociation energies are computed with the molecular species in its computed geometric minimum (a bromonium ion for $C_2H_4Br^+$). All calculations were performed for the anti isomer at the B3LYP/aug-cc-PVDZ level of theory.

to only a single photon (1.6 eV) is sufficient to strongly promote the fragmentation channel. The 320 fs time constant for Br• atom appearance is assigned to the elimination process, which must involve the motion of one Br atom towards the midpoint of the two carbon atoms, either in concert or in sequence with the elimination of the other Br atom. The dissociation lifetime does not change as a function of the excitation intensity (Fig. 4a), suggesting that the dissociation mechanism is not purely statistical, since in a statistical picture, extra energy should result in more rapid dissociation.[42]

In tandem with the appearance of the Br• atoms, we see a decaying signal with mirrored dynamics at around 65.3 eV (Fig. 5b). This spectral region includes the red tail of the molecular peaks we have attributed to DBE^+, however it also overlaps the location where a third Br• neutral peak should be visible. Since there is a possibility that atomic signals are contaminating this spectral window, we are reluctant to make any firm assignments as to the nature of the dynamics observed here. We note, however, that in TXA experiments on strong field ionized vinyl bromide, an electronically excited molecular cation was observed in a similar spectral region (65.5 eV), which decayed to produce Br• atoms. We assigned the peak around 65.7 eV to the first excited state of the DBE^+ ion, so it is possible, therefore, that the signal seen in Fig. 5b is evidence of decaying DBE^+ ions, in a similar manner.

4. Origin of Br^+ and Br^{++} fragments

Two different decay channels of strong-field ionized DBE to produce fragment Br^+ ions were found in VMI experiments:[16,17]

 This journal is © the Owner Societies 2016

Published on 11 May 2016. Downloaded by University of California - Berkeley on 27/05/2016 01:21:37.

a DI channel originating from DBE^+, and a Coulomb explosion (CE) channel originating from DBE^{++} (or higher charged) cations. The experimental appearance time of 70 fs for Br^+ production is consistent with direct dissociation upon a repulsive electronically excited state (DI);[36,37] conversely, it is faster than might be anticipated for statistical dissociation. Using a simple pseudo-diatomic classical model for Coulomb explosion of point charges, we can estimate a CE fragmentation time scale of 45 fs, taking 5 Å as the bond dissociation length (chosen because in calculations on CH_3Br, the potential energy surface on the C–Br stretch coordinate is flat at this distance[43]). This model uses the equilibrium bond length as the starting C–Br distance, and it assumes the charge is localized on the vacant C atom, which hence provides a lower bound for the dissociation time. CE reactions are thought to first incorporate a bond lengthening,[1,2] suggesting that in reality a slower CE time may be expected, so both DI and CE may fit the observed appearance time.

The DI and CE channels have different precursor molecular ions, so we can use the molecular transients to assign which dissociation mechanisms are observed. Fig. 5c shows the dynamics in the spectral window around 67 eV, which overlaps with the transient spectral feature assigned to the DBE^+ HOMO hole (see Fig. 3), while Fig. 5d shows the dynamics around 69 eV, overlapping the transient feature assigned to DBE^{++}. Note that as both windows are minima between atomic lines, we cannot conclusively rule out interference from atomic peaks in these dynamics, however there should still be significant contributions from the molecular features. Describing both transients using the 70 fs Br^+ rise time leads to an excellent fit for the DBE^+ (67 eV) transient (solid curve in c) and (within the signal-to-noise) acceptable agreement with the DBE^{++} (69 eV) trace (dashed curve in d). The excellent agreement with the DBE^+ transient suggests that we are observing a pronounced DI channel. At the intensities we have used, the CE channel is also expected to be present.[17] The acceptable fit to the DBE^{++} transient suggests this channel may also be contributing to the total Br^+ signal, albeit with a less clear signature than the DI channel. The rise of Br^+ products in our experiment can be well described using a single exponential rise function, so it appears both the DI and CE channels have a very similar lifetime, despite an entirely different mechanism. Alternatively, if the CE channel is relatively weak, then rapid CE dynamics may simply be obscured by a dominant DI channel.

The velocity map imaging studies by Wu *et al.* observed a significant yield of Br^{++} ions, but did not report their origin.[16,17] Similar to the Br^+ fragments, these could be born either from a DI channel from a DBE^{++} precursor, or a CE channel from a DBE^{+++} precursor. Our DFT calculations indicate that the DI channel requires significantly less energy than triple ionization of DBE (36 eV *vs.* 48 eV), however a DI channel would be in competition with the much more energetically favourable channel of CE leading to Br^+ elimination. The $\sim$30 fs lifetime is consistent with CE using a classical point charge model, described above. On the other hand, the decay of the DBE^{++} molecular transient feature located around 69 eV can be described with the Br^{++} rise time of 30 fs (Fig. 5d), suggesting that it could be dynamically linked to the Br^{++} production in a DI mechanism, although we are limited by poor signal-to-noise on this transient, along with the instrument response function. We do not explicitly observe a DBE^{+++} transient peak, although this is likely a limitation of the 72.5 eV upper bound of the spectrum we observe. Since the Br^{++} appearance time is similar to the experimental time resolution, we cannot be as definitive as with the $Br^\bullet$ and Br^+ cases. It is worth noting, however, that unlike $Br^\bullet$ and Br^+, the lifetime is on the order of the duration of the strong field excitation pulse. This means that the dynamics are not propagating in a field free regime, and instead strong perturbations both from the ponderomotive shift induced by the electric field of the pulse and coupling of states will play a role in a complex manner.[1,2,9] It is beyond the scope of this work to explore these very complex dynamics, however, on balance the most probable origin for the majority of Br^{++} ions is from a CE channel.

5. Effect of NIR Intensity and nature of dissociation channels

The effect of the NIR intensity is markedly different for the dynamics and the fragment yields. Considering the atomic Br^{n+} products, the charge distribution is increasingly skewed toward higher charge states as the NIR intensity increases. On the other hand, the dynamics that produce these atomic fragments are apparently unchanged by the incident field strength. For $Br^\bullet$ atoms produced from dissociative ionization of DBE^+, we can rationalize this observation by postulating that the 300 fs lifetime is dominated by the time required for nuclear motion leading to dissociation, which is independent of excitation energy. For Br^+, the dissociation mechanism appears to be a combination of CE and dissociation on a repulsive electronic surface, which is insensitive to excess internal energy, and Br^{++} likely appears from a rapid CE mechanism. It should be noted, however, that in these experiments we can only observe rapid early dynamics of the major channels. It is possible that there are also slower statistical channels operating on timescales beyond those explored in these experiments.

The overall picture is that as increasing energy is deposited, additional fragment atom/ion channels open up. Each additional level of ionization seems to be marked by a well-defined primary dissociation channel that leads to a free Br atom or ion. Within a given channel, increasing the strong field intensity has no effect on the dynamics. An important caveat is that the above arguments are all considering only the first Br dissociation event. In reality, the second Br atom may also be eliminated, which complicates the dynamics significantly. However, since simple monoexponential dynamics are able to reproduce the data well, we may presume that secondary dissociation is either a rare event or occurs on timescales well beyond 1 ps.

It is interesting to compare these results with previous strong field TXA experiments on dibromomethane[15] and vinyl bromide.[19] No Br^+ and Br^{++} fragments were observed in either of these experiments, in contrast to this work where they are major channels. Rather, $Br^\bullet$ atoms were the only atomic fragments observed, regardless of excitation pulse intensity. This a rather startling contrast, suggesting that either DBE has

Published on 11 May 2016. Downloaded by University of California - Berkeley on 27/05/2016 01:21:37.

unique dissociation properties compared to these molecules, or that experimental factors prevented charged atoms from being easily discerned in previous experiments. To our knowledge, no mass spectrometry of strong field ionized dibromomethane or vinyl bromide has been reported, which would give the most conclusive evidence for whether or not Br^+ is created. Alternatively, it is possible that variations in strong field intensity or laser pulse structure are sufficient to change product distributions. In both vinyl bromide and DBE, $Br^\bullet$ atoms appear in $\sim$320 fs, although in vinyl bromide, spin–orbit excited $Br^\bullet$ atoms were not observed. The similarity of time scales suggests that a similar mechanism for $Br^\bullet$ loss may be active in both systems. In vinyl bromide, $Br^\bullet$ atoms were associated with a spectral shift of a peak located at 65.5 eV, which was assigned as a HOMO$-$1 hole ionic state. The analogy with DBE is apparent: both involve an excited state decaying in field free conditions to give $Br^\bullet$ atoms on the same timescale. In the case of vinyl bromide, there was clear spectral evidence of the decaying ionic population, and in DBE a similar decay is observed, although the assignment of it is more tenuous. It is possible that the decay observed in DBE also belongs to a HOMO$-n$ hole, and the decay mechanism is very similar. In contrast, in dibromomethane, the timescales of $Br^\bullet$ formation were 75 fs and 130 fs, depending on the spin–orbit state of the product atom.[15] Clearly, the mechanism is radically different there from the vinyl bromide and DBE cases, suggesting that the addition of a second carbon atom plays an important role in the strong field excitation and relaxation dynamics.

Conclusions

We have performed femtosecond XUV transient absorption spectroscopy on 1,2-dibromoethane, following strong field ionization with an intense NIR pump pulse. Characteristic atomic Br 3d inner-shell absorption lines readily identify three channels for the formation of $Br^\bullet$, Br^+, and Br^{++} fragments. In line with expectations, increasing the NIR intensity skews the charge distribution in favor of higher charge states. On the other hand, the strong field intensity does not affect the dynamics in any of the dissociation channels. With NIR intensities ranging from 1.1×10^{13} to 2.2×10^{14} W cm^{-2}, the dynamics of Br^{n+} dissociation can be very well described by single exponential rise functions, with time constants τ_n of $\tau_0 = 320$ fs, $\tau_1 = 70$ fs and $\tau_2 = 30$ fs for the three charge states. Also visible are transient peaks associated with DBE^+ and DBE^{++}, which apparently decay by elimination of Br atoms in various charge states.

The neutral $Br^\bullet$ atom yield is already saturated at a NIR intensity of 7.5×10^{13} W cm^{-2}, and the most probable assignment for its origin is dissociative ionization involving vibrationally excited DBE^+ ions marked by a shallow potential well along the $Br^\bullet$ elimination coordinate. Note that the ability to track neutral fragments in conjunction with charged fragments is unique to the TXA methodology. Singly charged Br^+ ions likely appear from a combination of a dissociative ionization mechanism on a repulsive electronic state of DBE^+ and Coulomb explosion of DBE^{++}. Experimental evidence for dissociative ionization comes in the form of a molecular transient assigned to DBE^+, which decays with the same time constant as the Br^+ fragments appear. Br^{++} dications are produced within the duration of the exciting laser pulse, presumably from either dissociative ionization, or Coulomb explosion of highly charged DBE ions. In all three cases, an excited ion decays by release of a Br atom.

Acknowledgements

This work was supported by the U. S. Department of Energy, Office of Basic Energy Sciences, Chemical Sciences, Geosciences and Biosciences Division, through Contract No. DE-AC02-05CH11231. F. L. would like to acknowledge support by the Austrian Science Fund (FWF, Erwin Schrödinger Fellowship Grant No. J 3580-N20). We would like to thank Chaitanya D. Pemmaraju for assistance with the DFT calculations.

References

1 R. J. Levis and M. J. DeWitt, *J. Phys. Chem. A*, 1999, **103**, 6493–6507.
2 J. H. Posthumus, *Rep. Prog. Phys.*, 2004, **67**, 623.
3 A. E. Boguslavskiy, J. Mikosch, A. Gijsbertsen, M. Spanner, S. Patchkovskii, N. Gador, M. J. J. Vrakking and A. Stolow, *Science*, 2012, **335**, 1336–1340.
4 M. Lezius, V. Blanchet, D. M. Rayner, D. M. Villeneuve, A. Stolow and M. Y. Ivanov, *Phys. Rev. Lett.*, 2001, **86**, 51–54.
5 M. Kotur, T. C. Weinacht, C. Zhou, K. A. Kistler and S. Matsika, *J. Chem. Phys.*, 2011, **134**, 184309.
6 M. Kotur, T. C. Weinacht, C. Zhou and S. Matsika, *Phys. Rev. X*, 2011, **1**, 021010.
7 S. Chelkowski and A. D. Bandrauk, *J. Phys. B: At., Mol. Opt. Phys.*, 1995, **28**, L723.
8 H. Stapelfeldt, E. Constant and P. B. Corkum, *Phys. Rev. Lett.*, 1995, **74**, 3780–3783.
9 A. N. Markevitch, S. M. Smith, D. A. Romanov, H. Bernhard Schlegel, M. Y. Ivanov and R. J. Levis, *Phys. Rev. A: At., Mol., Opt. Phys.*, 2003, **68**, 011402.
10 J. J. Macklin, J. D. Kmetec and C. L. Gordon, *Phys. Rev. Lett.*, 1993, **70**, 766–769.
11 M. Lewenstein, P. Balcou, M. Y. Ivanov, A. L'Huillier and P. B. Corkum, *Phys. Rev. A: At., Mol., Opt. Phys.*, 1994, **49**, 2117–2132.
12 Z. Chang, A. Rundquist, H. Wang, M. M. Murnane and H. C. Kapteyn, *Phys. Rev. Lett.*, 1997, **79**, 2967–2970.
13 D. Geißler, B. J. Pearson and T. Weinacht, *J. Chem. Phys.*, 2007, **127**, 204305.
14 B. J. Pearson, S. R. Nichols and T. Weinacht, *J. Chem. Phys.*, 2007, **127**, 131101.
15 Z.-H. Loh and S. R. Leone, *J. Chem. Phys.*, 2008, **128**, 204302.
16 H. Wu, Y. Yang, S. Sun, J. Zhang, L. Deng, S. Zhang, T. Jia, Z. Wang and Z. Sun, *Chem. Phys. Lett.*, 2014, **607**, 70–74.

 This journal is © the Owner Societies 2016

Published on 11 May 2016. Downloaded by University of California - Berkeley on 27/05/2016 01:21:37.

17 H. Wu, S. Zhang, Y. Yang, S. Sun, J. Zhang, L. Deng, T. Jia, Z. Wang and Z. Sun, *RSC Adv.*, 2014, **4**, 45300–45305.
18 Y. Yang, L. Fan, S. Sun, J. Zhang, Y. Chen, S. Zhang, T. Jia and Z. Sun, *J. Chem. Phys.*, 2011, **135**, 064303.
19 M.-F. Lin, D. M. Neumark, O. Gessner and S. R. Leone, *J. Chem. Phys.*, 2014, **140**, 064311.
20 A. Assion, T. Baumert, M. Bergt, T. Brixner, B. Kiefer, V. Seyfried, M. Strehle and G. Gerber, *Science*, 1998, **282**, 919–922.
21 J. Plenge, A. Wirsing, I. Wagner-Drebenstedt, I. Halfpap, B. Kieling, B. Wassermann and E. Ruhl, *Phys. Chem. Chem. Phys.*, 2011, **13**, 8705–8714.
22 T. Ergler, A. Rudenko, B. Feuerstein, K. Zrost, C. D. Schröter, R. Moshammer and J. Ullrich, *Phys. Rev. Lett.*, 2006, **97**, 193001.
23 J. L. Hansen, J. H. Nielsen, C. B. Madsen, A. T. Lindhardt, M. P. Johansson, T. Skrydstrup, L. B. Madsen and H. Stapelfeldt, *J. Chem. Phys.*, 2012, **136**, 204310.
24 Z.-H. Loh and S. R. Leone, *J. Phys. Chem. Lett.*, 2013, **4**, 292–302.
25 A. R. Attar, A. Bhattacherjee and S. R. Leone, *J. Phys. Chem. Lett.*, 2015, **6**, 5072–5077.
26 Z.-H. Liu, Y.-Q. Wang, J.-J. Ma, L. Wang and G.-Z. He, *Chem. Phys. Lett.*, 2004, **383**, 198–202.
27 M.-F. Lin, A. N. Pfeiffer, D. M. Neumark, S. R. Leone and O. Gessner, *J. Chem. Phys.*, 2012, **137**, 244305.
28 S. M. Hankin, D. M. Villeneuve, P. B. Corkum and D. M. Rayner, *Phys. Rev. A: At., Mol., Opt. Phys.*, 2001, **64**, 013405.
29 Y. Shao, Z. Gan, E. Epifanovsky, A. T. B. Gilbert, M. Wormit, J. Kussmann, A. W. Lange, A. Behn, J. Deng, X. Feng, D. Ghosh, M. Goldey, P. R. Horn, L. D. Jacobson, I. Kaliman, R. Z. Khaliullin, T. Kuś, A. Landau, J. Liu, E. I. Proynov, Y. M. Rhee, R. M. Richard, M. A. Rohrdanz, R. P. Steele, E. J. Sundstrom, H. L. Woodcock, P. M. Zimmerman, D. Zuev, B. Albrecht, E. Alguire, B. Austin, G. J. O. Beran, Y. A. Bernard, E. Berquist, K. Brandhorst, K. B. Bravaya, S. T. Brown, D. Casanova, C.-M. Chang, Y. Chen, S. H. Chien, K. D. Closser, D. L. Crittenden, M. Diedenhofen, R. A. DiStasio, H. Do, A. D. Dutoi, R. G. Edgar, S. Fatehi, L. Fusti-Molnar, A. Ghysels, A. Golubeva-Zadorozhnaya, J. Gomes, M. W. D. Hanson-Heine, P. H. P. Harbach, A. W. Hauser, E. G. Hohenstein, Z. C. Holden, T.-C. Jagau, H. Ji, B. Kaduk, K. Khistyaev, J. Kim, J. Kim, R. A. King, P. Klunzinger, D. Kosenkov, T. Kowalczyk, C. M. Krauter, K. U. Lao, A. D. Laurent, K. V. Lawler, S. V. Levchenko, C. Y. Lin, F. Liu, E. Livshits, R. C. Lochan, A. Luenser, P. Manohar, S. F. Manzer, S.-P. Mao, N. Mardirossian, A. V. Marenich, S. A. Maurer, N. J. Mayhall, E. Neuscamman, C. M. Oana, R. Olivares-Amaya, D. P. O'Neill, J. A. Parkhill, T. M. Perrine, R. Peverati, A. Prociuk, D. R. Rehn, E. Rosta, N. J. Russ, S. M. Sharada, S. Sharma, D. W. Small, A. Sodt, T. Stein, D. Stück, Y.-C. Su, A. J. W. Thom, T. Tsuchimochi, V. Vanovschi, L. Vogt, O. Vydrov, T. Wang, M. A. Watson, J. Wenzel, A. White, C. F. Williams, J. Yang, S. Yeganeh, S. R. Yost, Z.-Q. You, I. Y. Zhang, X. Zhang, Y. Zhao, B. R. Brooks, G. K. L. Chan, D. M. Chipman, C. J. Cramer, W. A. Goddard, M. S. Gordon, W. J. Hehre, A. Klamt, H. F. Schaefer, M. W. Schmidt, C. D. Sherrill, D. G. Truhlar, A. Warshel, X. Xu, A. Aspuru-Guzik, R. Baer, A. T. Bell, N. A. Besley, J.-D. Chai, A. Dreuw, B. D. Dunietz, T. R. Furlani, S. R. Gwaltney, C.-P. Hsu, Y. Jung, J. Kong, D. S. Lambrecht, W. Liang, C. Ochsenfeld, V. A. Rassolov, L. V. Slipchenko, J. E. Subotnik, T. Van Voorhis, J. M. Herbert, A. I. Krylov, P. M. W. Gill and M. Head-Gordon, *Mol. Phys.*, 2015, **113**, 184–215.
30 R. A. Kendall, T. H. Dunning and R. J. Harrison, *J. Chem. Phys.*, 1992, **96**, 6796–6806.
31 A. K. Wilson, D. E. Woon, K. A. Peterson and T. H. Dunning, *J. Chem. Phys.*, 1999, **110**, 7667–7676.
32 A. P. Hitchcock and C. E. Brion, *J. Electron. Spectrosc. Relat. Phenom.*, 1978, **13**, 193–218.
33 K. H. Sze, C. E. Brion and A. Katrib, *Chem. Phys.*, 1989, **132**, 271–293.
34 A. Cummings and G. O'Sullivan, *Phys. Rev. A: At., Mol., Opt. Phys.*, 1996, **54**, 323–334.
35 F. Lackner, A. S. Chatterley, C. D. Pemmaraju, K. D. Closser, D. Prendergast, D. M. Neumark, S. R. Leone, O. Gessner, in preparation, 2016.
36 M. E. Vaida and S. R. Leone, *Chem. Phys.*, 2014, **442**, 41–47.
37 A. S. Mereshchenko, E. V. Butaeva, V. A. Borin, A. Eyzips and A. N. Tarnovsky, *Nat. Chem.*, 2015, **7**, 562–568.
38 R. H. Staley, R. D. Wieting and J. L. Beauchamp, *J. Am. Chem. Soc.*, 1977, **99**, 5964–5972.
39 D. W. Berman, V. Anicich and J. L. Beauchamp, *J. Am. Chem. Soc.*, 1979, **101**, 1239–1248.
40 R. A. Poirier, G. R. Demaré, K. Yates and I. G. Csizmadia, *THEOCHEM*, 1983, **94**, 137–141.
41 J. L. Holmes, F. P. Lossing and R. A. McFarlane, *Int. J. Mass Spectrom. Ion Processes*, 1988, **86**, 209–215.
42 T. Baer and W. L. Hase, *Unimolecular reaction dynamics: theory and experiments*, Oxford University Press, New York, 1996.
43 C. Escure, T. Leininger and B. Lepetit, *J. Chem. Phys.*, 2009, **130**, 244305.